sPHENIX Report

tag: sPH-TRIG-2023-001
version: 0.1
DOI: unspecified
date: August 23, 2023

Early investigation of the MVTX commissioning

Jaehyun Kim (Yonsei University) for the sPHENIX MVTX group

Abstract

We make an early diagnosis of the data collected in the MVTX commissioning, collect a few indicators for the successful operation of the detector, and identify the next milestones for the operation of the detector and the analysis of the resulting data.

1 Introduction

We investigated the data relevant to the MVTX detector collected during the commissioning. We inspected the operation including noise filter and threshold setting through the studies on the clusters to be detailed in the text and simple particle trajectory reconstruction. Some studies were also conducted for the backgrounds irrelevant to the real collisions, which will affect the detector operation. We identified milestones for the next step, improving the quality of the detector alignment, extending the trajectory reconstruction capability, and detailing the efficiency of the detector.

2 Data

We used the data in the reference [1], which has yielded approved Figure 1 and Figure 2 reproduced here again for the convenient discussion.

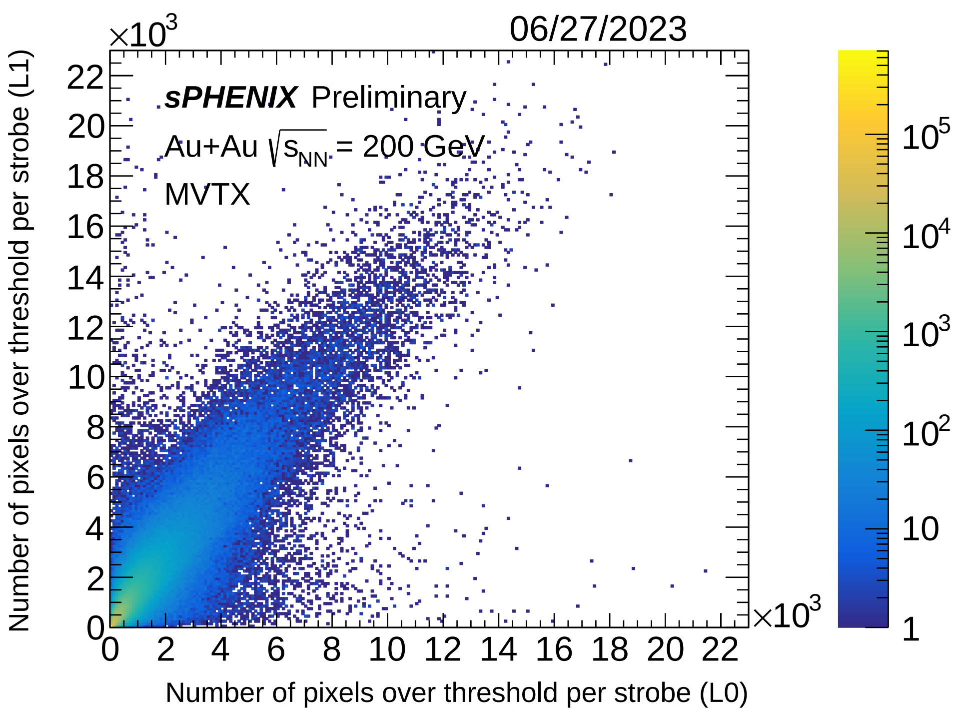

Figure 1: MVTX internal correlation of the number of pixel hits over thresholds per strobe between the two staves (L0_01 and L0_02) in layer 0 and the three staves (L1_01, L1_02, and L1_03) in layer 1.

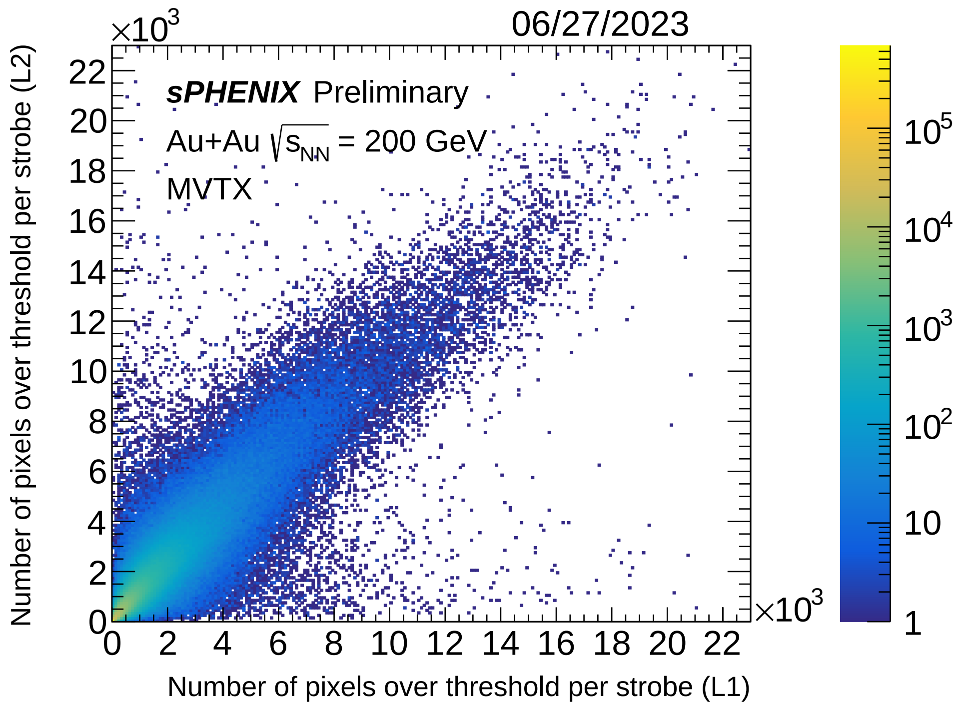

Figure 2: MVTX internal correlation of the number of pixel hits over thresholds per strobe between the three staves (L1_01, L1_02, and L1_03) in layer 1 and the four staves (L2_01, L2_02, L2_03, and L2_04) in layer 2.

2.1 Location of PRDF

```
dir=/sphenix/lustre01/sphnxpro/commissioning/MVTX/data/runs
  $dir/MVTX_FLX0/20230627-145225_FelixFakeHitRate/mvtx_mvtxflx0000201240000.evt
  $dir/MVTX_FLX1/20230627-145227_FelixFakeHitRate/mvtx_mvtxflx1000201240000.evt
  $dir/MVTX_FLX2/20230627-145225_FelixFakeHitRate/mvtx_mvtxflx2000201240000.evt
  $dir/MVTX_FLX3/20230627-145225_FelixFakeHitRate/mvtx_mvtxflx3000201240000.evt
  $dir/MVTX_FLX4/20230627-145225_FelixFakeHitRate/mvtx_mvtxflx4000201240000.evt
  $dir/MVTX_FLX5/20230627-145225_FelixFakeHitRate/mvtx_mvtxflx5000201240000.evt
```

3 Cluster characteristics

It is expected that typical charged particles are supposed to create a few consecutively firing pixels in a given ALPIDE sensor[2]. We defined the cluster as the consecutively firing pixels grouped together.

3.1 Significant number of clusters have large sizes

We note the clusters with large numbers of the associated pixels explain the large numbers of firing pixels beyond 10,000 in the detector layers.

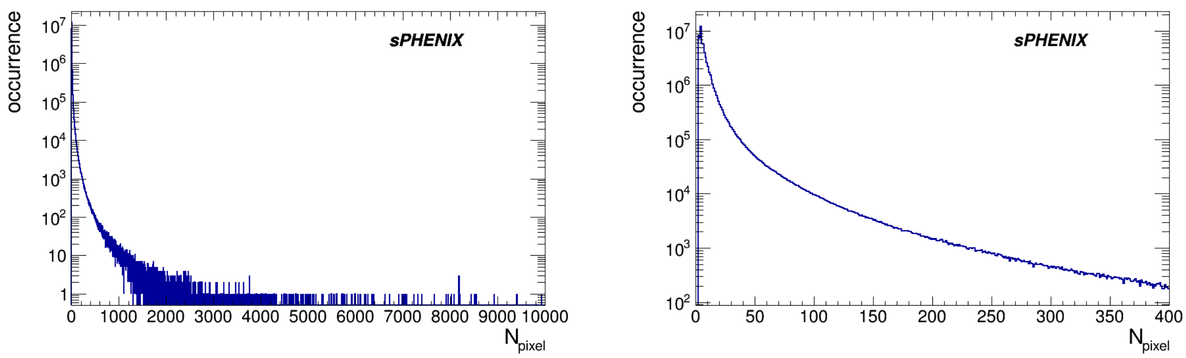

Figure 3: Cluster size distribution after removing hot pixels.

We suspect these large clusters are the backgrounds from the upstream beam interaction with the following considerations.

- There were low ZDC coincidence rates(100Hz) relative to the strobe rates(11,000Hz), but most of the readout frames have large number of firing pixels. Therefore, most of the recorded data are irrelevant to collision.

- There are many clusters with large sizes for most of the readout frames, and these large clusters seems to have physical origin, possibly caused by the upstream beam interaction, when we consider the firing pixel patterns.

- Very large clusters will stress readout with occupancy and cause failures, which might explain some difficulties in the MVTX operation.

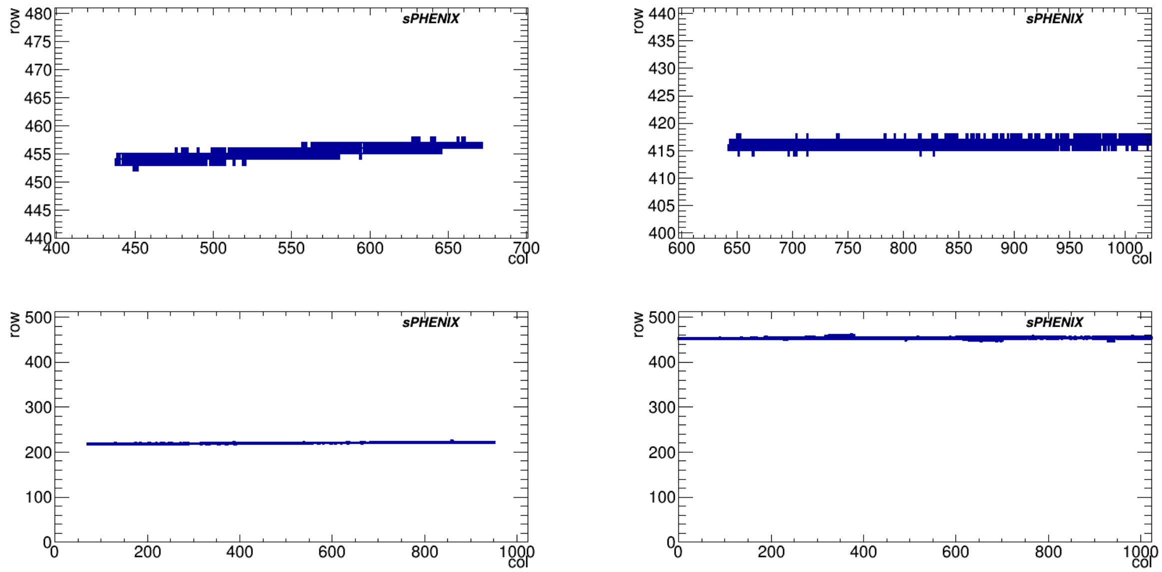

Figure 4: A few examples with large cluster size.

3.2 Most frequent cluster patterns have 4 or less pixels firing

The clusters have typical patterns shown in Figure 5, which are similar to the previous application of the sensor in the ALICE experiment[2]. These patterns are used to define the normal clusters corresponding to about 55% of the whole clusters. In addition, normal clusters have the global positions calculated from the associated pixel positions by the center of gravity.

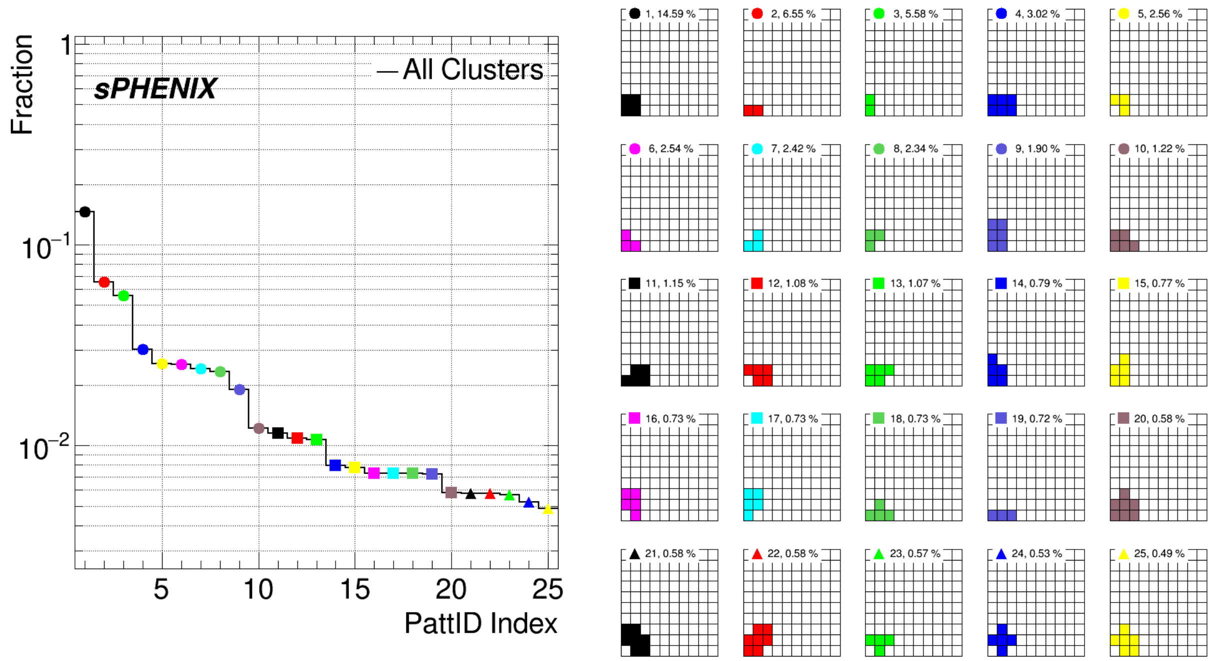

Figure 5: Left plot shows distribution of cluster pattern and right top 25 sub-plots show each cluster pattern.

Distributions of the normal cluster numbers in the layer 0, 1, and 2 per event, $N_{cl,0}$, $N_{cl,1}$, and $N_{cl,2}$ have distinctive peaks near zero and long tails towards large number. We noted approximately 50% of the readout frames have small number of normal clusters in the layer 0, 1, and 2 as shown in Figure 6. We classified these readout frames without the real collision event.

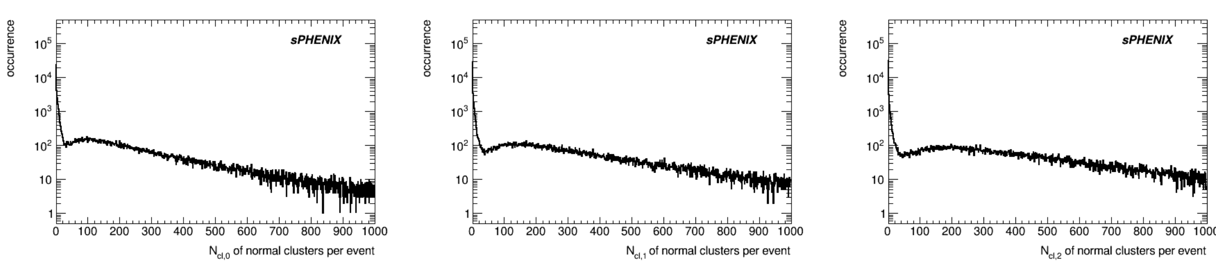

Figure 6: Number of normal clusters per event at layer 0, 1, and 2, respectively.

Approximately 50% of the readout frames have small numbers, specifically 12, of normal clusters in the layer 0, 1, and 2. We identified these as the empty events. The number of clusters in the layer 0, 1, and 2 show a good correlation. Distribution of the total number of clusters has a peak near 400 and a long tail beyond 10,000.

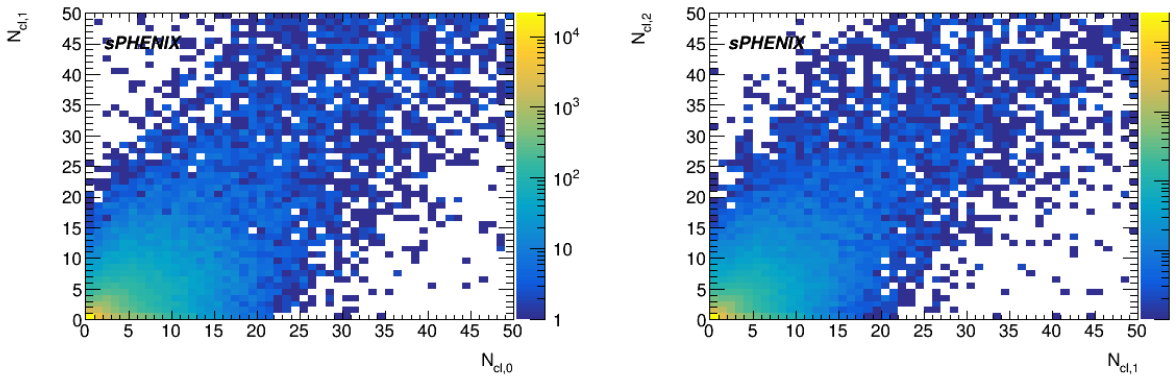

Figure 7: Correlation in the numbers of normal clusters in the layer 0, 1, and 2.

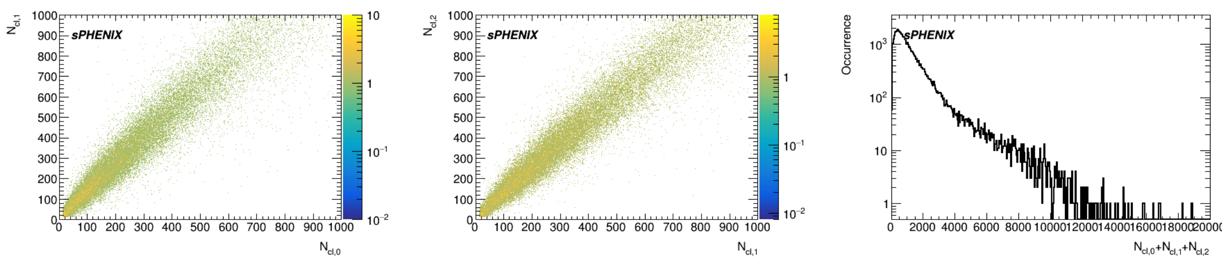

Figure 8: The left two : correlation between the number of the normal clusters excluding empty events, the right most : total number of the normal clusters.

4 Crude tracking

We scanned 100,000 strobes ($\sim$ 1000 ZDC coincidence) from the RUN specified above and discarded empty events classified above.

We assumed

- three consecutive hits in the layer 0, 1 and 2(perfect efficiency),

- there are poor but approximate detector alignment(sufficiently large search window),

- particle trajectories are straight line within the given limitation,

- and collisions occurred along the nominal collision axis.

We selected low occupancy events or peripheral events $(N_{cl,2} < 50)$ to ensure sufficient granularity of the detector to verify the coincidence of hits and to reconstruct the particle trajectories. At the end of exercises, we selected and displayed handful of probable collision events and verified the qualitative performance of the MVTX detector in this first exploratory investigation.

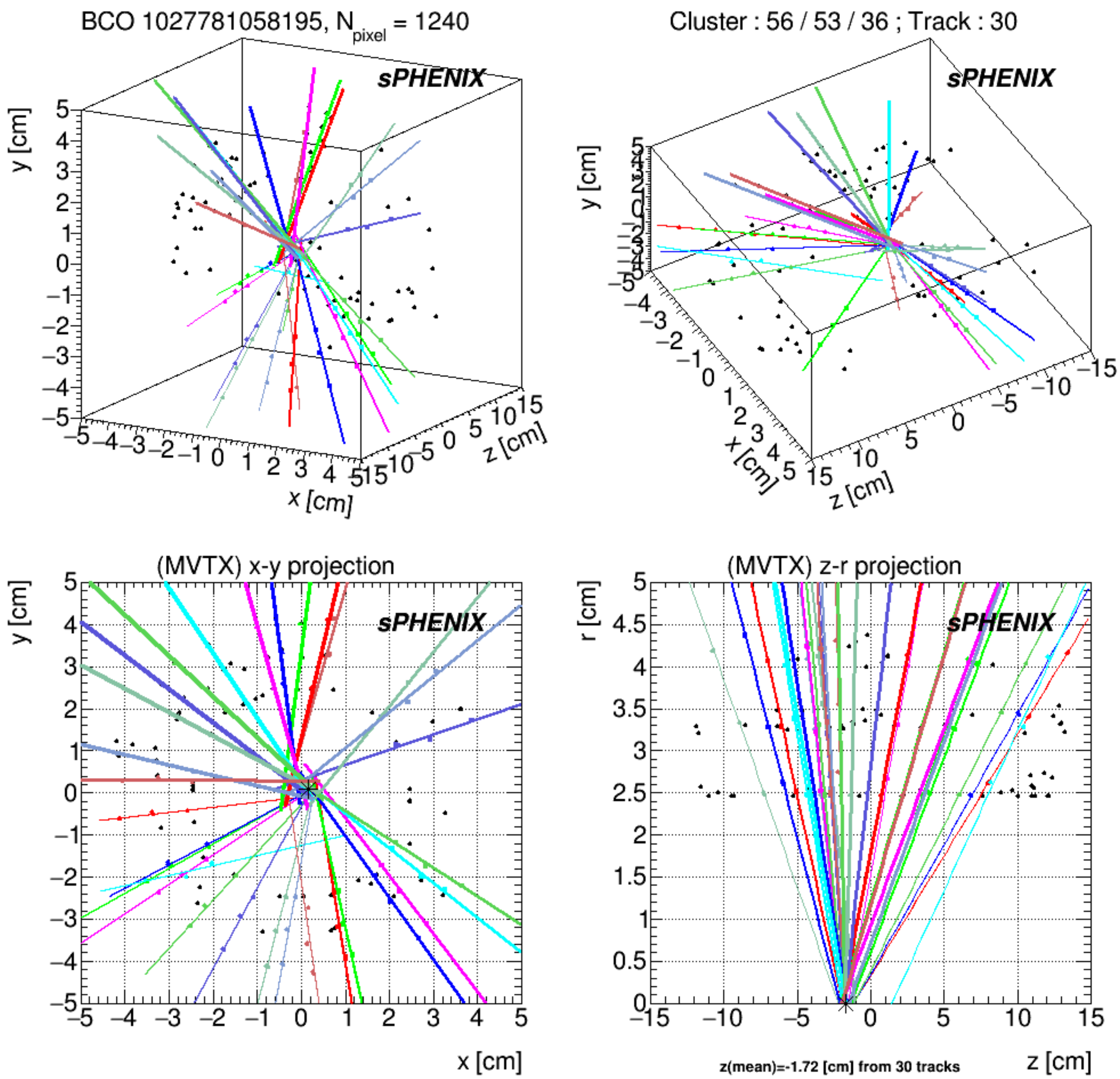

Figure 9: The event display for one single event. Top left and right are two different 3D views. Bottom left is the xy projection and bottom right is the zr projection.(example 1)

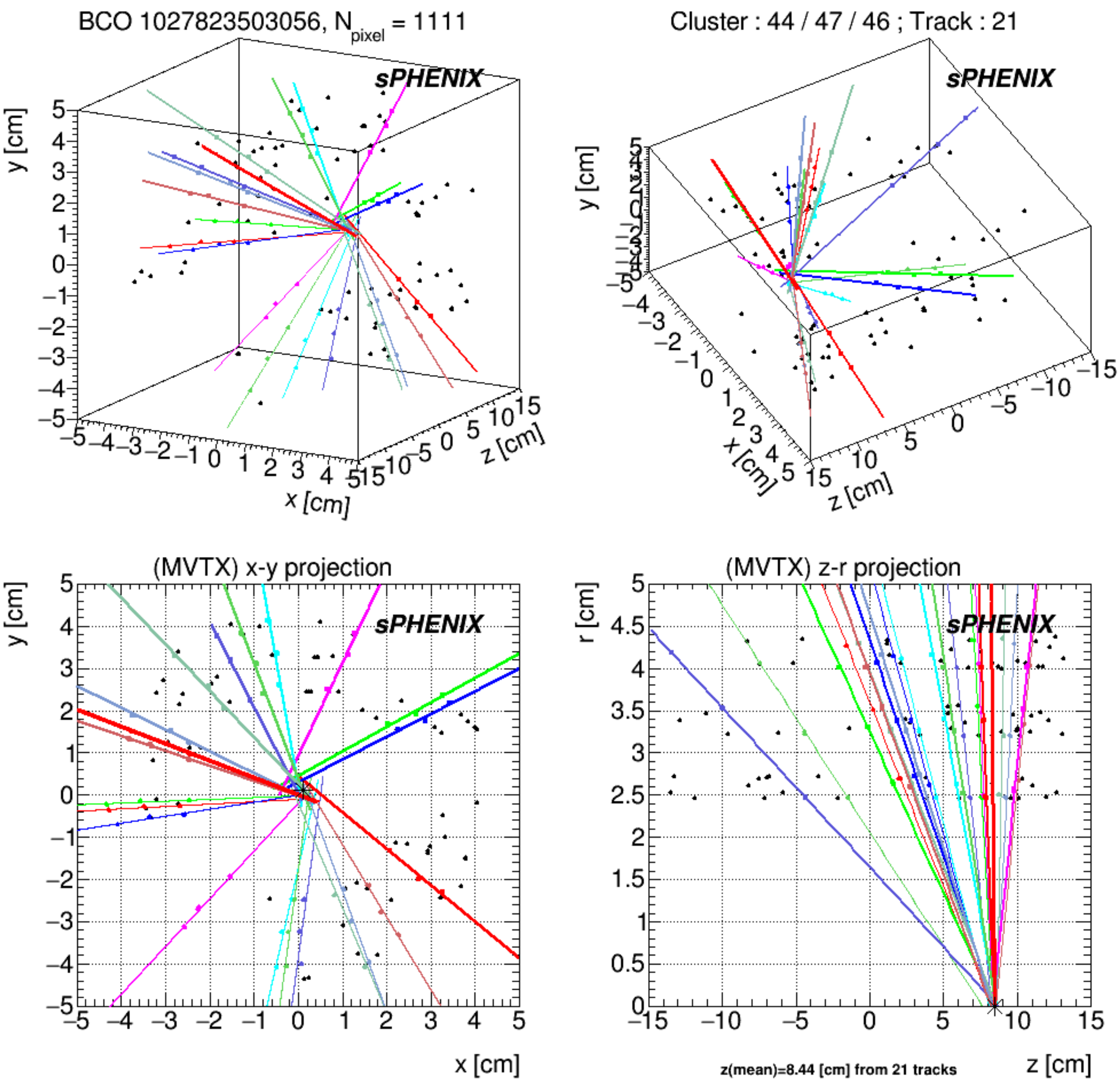

Figure 10: The event display for one single event. Top left and right are two different 3D views. Bottom left is the xy projection and bottom right is the zr projection.(example 2)

6 Summary and Outlook

We performed a quick diagnostics to verify 267 trajectories found from 12 selected events. Figure 11 shows the distribution of deviations Δ_Z and Δ_{XY} from the straight line assumption, defined as follows using the nominal position(x_L, y_L, z_L) of the clusters in the layer L =0, 1, and 2. Generous search window for the coincident hits appears with a substantial spread of the distribution. However, most of the trajectories exhibit the expected behavior as well as small mismatch.

While the distribution of Δ_Z is centered around zero with the spread of about 80 μm, the one of Δ_{XY} has a peak with the spread of about 160 μm at an offset of about 650 μm. The observed shift of the peak will be due to the misalignment among the detector layers. Wider spread of the peak in the same distribution can be due to the deflection of the particle trajectories in the magnetic field or misalignment.

The obvious nest milestone will be the improved alignment of the detector and extension of the analyzed event centrality class, which might lead to the physics measurements.

$$\Delta_Z = z_{1,projected} \text{ - } z_1 \text{ and } \Delta_{XY} = \phi_{1,projected}\sqrt{x^2_{1,projected} + y^2_{1,projected}} \text{ - } \phi_1\sqrt{x_1^2 + y_1^2}$$

where

$$x_{1,projected} = x_2 \text{ - } (x_0 - x_2)^2(x_2 - x_1) \ / \ \sqrt{(x_0 - x_2)^2 + (y_0 - y_2)^2 + (z_0 - z_2)^2},$$

$$y_{1,projected} = y_2 \text{ - } (y_0 - y_2)^2(y_2 - y_1) \ / \ \sqrt{(x_0 - x_2)^2 + (y_0 - y_2)^2 + (z_0 - z_2)^2},$$

$$z_{1,projected} = z_2 \text{ - } (z_0 - z_2)^2(z_2 - z_1) \ / \ \sqrt{(x_0 - x_2)^2 + (y_0 - y_2)^2 + (z_0 - z_2)^2},$$

$$\phi_{1,projected} = \tan^{-1}(y_{1,projected}/x_{1,projected}),$$

and $\phi_1 = \tan^{-1}(y_1/x_1)$.

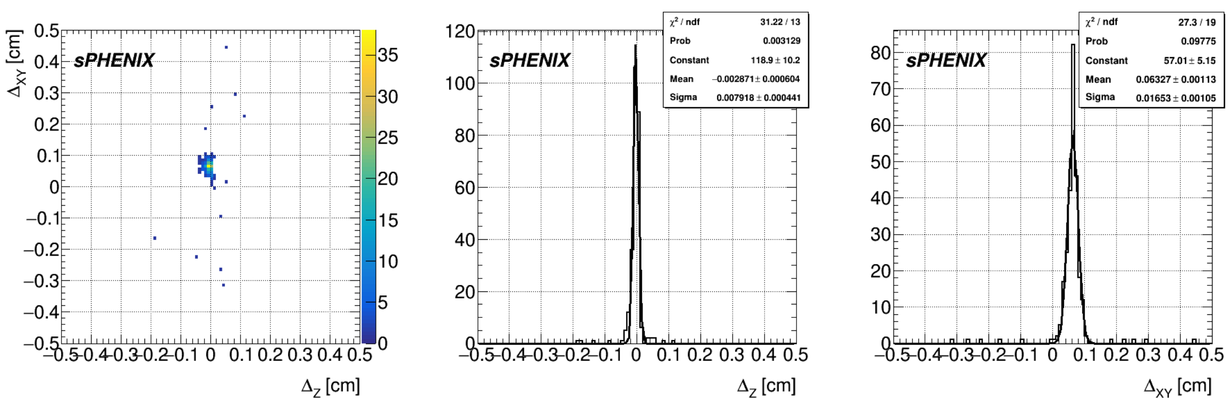

Figure 11: The first plot shows Δ_{XY} vs Δ_Z, the second one shows Δ_Z and the last one shows Δ_{XY} distribution.

As a study for the improvement of the detector operation, we investigated the large clusters possibly caused by the upstream beam interaction in a few ways. Correlations in the number of very large are shown in Figure 12. These large clusters will be caused by the shallow particles. Occurrences of the large clusters are harmful to the sensor. Simultaneous occurrence of the large clusters will burden the sensor readout and might cause failures in data acquisition. Suppression of the beam interaction outside the nominal collision zone is likely to reduce these shallow trajectories.

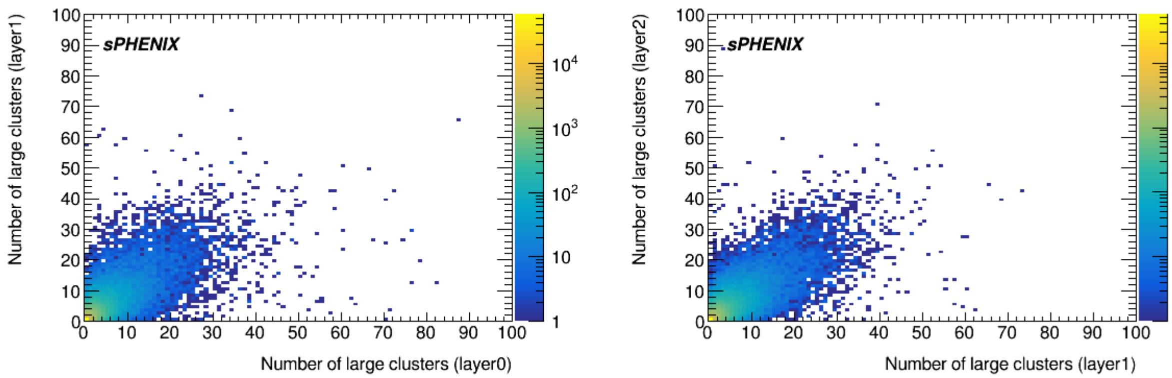

Figure 12: Correlation in the numbers of very large clusters ($N_{pixel} > 100$) in the layer 0, 1, and 2.

References

[1] Hao-Ren Jheng (MIT) on behalf of the sPHENIX MVTX group. MVTX internal staves correlation. 2023. (document)

[2] M. Mager (CERN) On behalf of the ALICE Collaboration. ALPIDE, the Monolithic Active Pixel Sensor for the ALICE ITS upgrade. *Nucl. Instrum. Meth.*, 824:434–438, 2016. doi: 10.1016/j.nima.2015.09.057. (document)